PRE-BUCKLING IMPERFECTION SENSITIVITY OF PULTRUDED FRP PROFILES

Luigi Ascione (corresponding author)

Department of Civil Engineering, University of Salerno,

Via Giovanni Paolo II, 84084, Fisciano (SA) ITALY, e-mail: l.ascione@unisa.it

Valentino Paolo Berardi

Department of Civil Engineering, University of Salerno,

Via Giovanni Paolo II, 84084, Fisciano (SA) ITALY, e-mail: berardi@unisa.it

Antonella Giordano

Department of Civil Engineering, University of Salerno,

Via Giovanni Paolo II, 84084, Fisciano (SA) ITALY, e-mail: angiordano@unisa.it

Saverio Spadea

Department of Civil Engineering, University of Salerno,

Via Giovanni Paolo II, 84084, Fisciano (SA) ITALY, e-mail: sspadea@unisa.it

Abstract

This paper presents a geometrically non-linear one-dimensional model suitable for analyzing thin-walled fiber-reinforced polymer profiles, which accounts for the effect of manufacturing imperfections. The kinematic model is developed under the hypotheses of small strains and moderately large rotations of the cross-sections, and is able to take into consideration the contribution of shear strains and the effects related to warping displacements.

The aim of the study is to develop a proper tool to analyze the pre-buckling behavior of such beams, since current approaches based on two-dimensional finite element method analysis demand significant computational efforts to be applied to real structures. The numerical results underline the effectiveness of the proposed mechanical model in analyzing case studies of technical interest in Civil Engineering, and the relevant influence of geometrical imperfections on the structural performance of FRP components with regard to serviceability design requirements.

Keywords

B. Buckling

B. Defects

C. Numerical analysis

E. Pultrusion

1. Introduction

Pultruded fiber reinforced polymer (PFRP) profiles are characterized by very slender proportions due to their high strength and relatively low stiffness combined with low density. Therefore, the design of all-PFRP structures is usually controlled by buckling behavior as opposed to material strength. In addition, the thin-walled beam cross-section and low shear stiffness of the composite materials may affect the ultimate behavior of PFRP beams, which is typically characterized by either local or global buckling.

Numerous experimental, theoretical and numerical studies dealing with the influence of shear deformation on the global and local buckling behavior of PFRP beams are available in current literature [1]-[7]. With reference to the non-linear behavior of thin-walled composite beams, a number of suitable mechanical models were proposed by several researchers [8]-[11]. However,

these investigations do not examine the serviceability design implications related to the high deformability of composite materials.

On this topic, Nguyen et al. [12] studied, through FEM and orthotropic plate elements based on Mindlin's theory, the lateral torsional buckling resistance of composite I-beams in consideration of initial geometrical imperfections. Moreover, Laudiero et al. [14] investigated the imperfection sensitivity of PFRP profiles in pure compression. Both studies were performed with the aim of analyzing the pre-buckling behavior of thin-walled composite beams and collecting results useful for practical purposes. However, these approaches cannot be easily applied to real structures (e.g., all-PFRP frames or trusses) due to computational complexity, as they are based on two-dimensional FEM analysis. Ascione and Mancusi [15] and Ascione [16] proposed a mechanical model based on the subdivision of cross section into interconnected thin sub-components, each one analyzed on the basis of the classical Timoshenko beam theory. In this case, an approximation of warping effects is given by the relative displacements among the different sub-components.

Therefore, within the context of structural design at Serviceability Limit States, further and effective models are required in order to give more expedient and quick computational tools useful for designers and able to consider the effects of warping displacements variation on the cross-section.

In this paper, the authors present a one-dimensional non-linear mechanical model formulated by extending Vlasov's theory to composite beams and capable of predicting the pre-buckling behavior of imperfect PFRP beams with open thin-walled cross-sections. The mechanical model takes into account the contribution of shear deformation in the kinematic hypotheses under the assumption of small strains and moderate rotations.

Moreover, a FEM code was implemented in order to study the mechanical behavior of typical PFRP I-beams loaded in bending with initial geometric imperfection. Different values for the beam slenderness and imperfection amplitude are considered in order to study in-depth the imperfection sensitivity on pre-buckling behavior.

2. Kinematics

The kinematics of a straight thin-walled beam with a constant cross-section is taken into consideration (Figure 1a). The cross-section is defined by its middle line $\rho(s)$ and thickness $b(s)$, with s being a curvilinear abscissa with its origin in a generic point M of $\rho(s)$ (Figure 1b).

Two different reference frames were introduced into the analytical developments that follow. The global reference frame $\{\mathrm{G}, \mathbf{i}, \mathbf{j}, \mathbf{k}\}$ has its origin in the centroid of the Σ_0 cross section: the x and y axes coincide with the principal axes of inertia, while the z axis coincides with the axis of the beam. The local reference frame $\{\mathrm{P}, \mathbf{n}, \mathbf{t}, \mathbf{k}\}$ has its origin in a generic point on the cross-section of the middle line curve $\rho(s)$: the unit vectors $\mathbf{n}$ and $\mathbf{t}$ are respectively normal and tangent to $\rho(s)$ (Figure 1b).

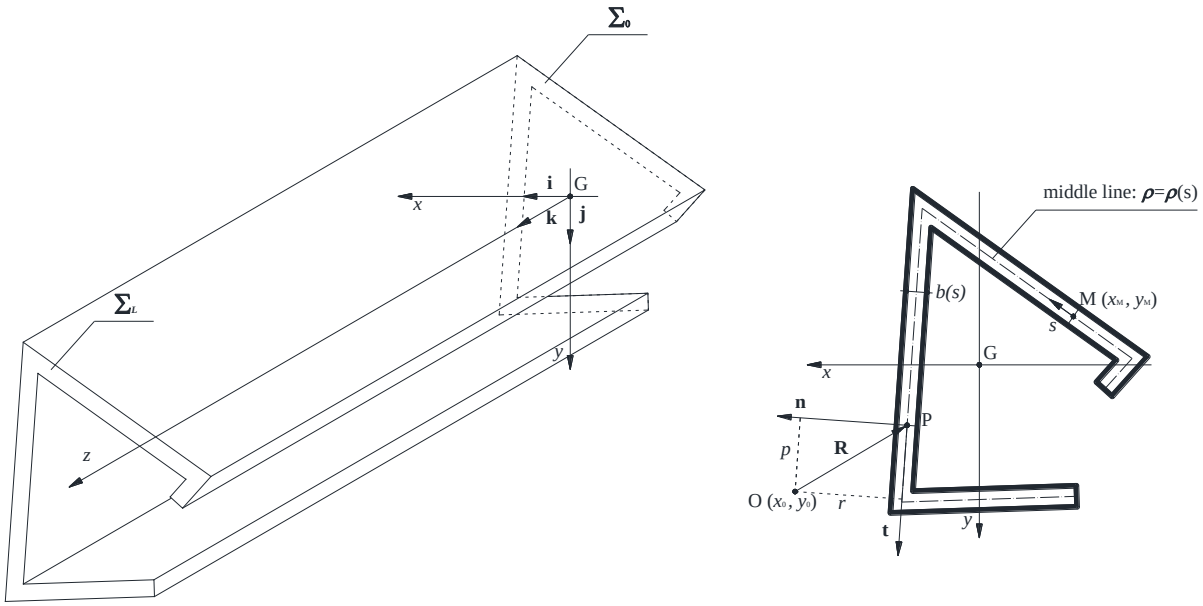

(a) (b)

Figure 1 – Thin-walled beam: a) Global reference frame and displacement field; b) Cross-section and local reference frame.

The present non-linear formulation is based on the assumptions of small strains and moderate rotations. The beam cross-section is assumed to be undeformable in its own plane. It is also assumed that the beam cross-section does not remain plane in the deformed configuration due to warping displacements. Since the changes in geometry are small, no distinction between the second Piola-Kirchhoff and Cauchy stress tensors is considered. The composite material is assumed to be linear-elastic, homogeneous, and transversely isotropic, with the isotropy plane coincident with the cross-section plane of the beam. Moreover, the thin-walled geometry allows us to neglect the shear strains between the n and z axes.

Accordingly, the displacement components, u, v and w, of the generic point of the beam in the global reference system (Figure 1a) can be expressed as follows:

$$u = u(x, y, z) = u_0(z) - \varphi_0(z)\left(y - y_0\right), \tag{1a}$$

$$v = v(x, y, z) = v_0(z) + \varphi_0(z)\left(x - x_0\right), \tag{1b}$$

$$w = w(x, y, z) = \varphi_x(z)\left(y - y_M\right) - \varphi_y(z)\left(x - x_M\right) + \bar{w}(x, y, z)\,. \tag{1c}$$

Equations (1a,b,c) express the displacement field of the beam in terms of:

- the rotations φ_0 around the arbitrary pole, O, lying in the cross-section plane (Figure 1b);
- the displacements of the pole in the x and y directions, u_0 and v_0, respectively;
- the component $\bar{w}$ of the warping displacement along the z axis;
- the rotations φ_x and φ_y around the two axes intersecting at the point M and parallel to the x and y axes.

To understand the role of warping in deriving the Green-Saint Venant strain tensor, additional approximations are performed beginning with the infinitesimal shear strain component $\varepsilon_{tz}(n, s, z)$ in the local reference frame $\{\mathrm{P}, \mathbf{n}, \mathbf{t}, \mathbf{k}\}$. While considering the thin-walled geometry and introducing a first-order MacLaurin approximation, it is possible to represent $\varepsilon_{tz}(n, s, z)$, as follows (see [4]):

$$\varepsilon_{tz}(n, s, z) = \varepsilon_{tz}(0, s, z) + \left.\frac{\partial \varepsilon_{tz}}{\partial n}\right|_{n=0} n = \frac{1}{2}\left[\left(u_0' - \varphi_y\right)\frac{dx}{ds} + \left(v_0' + \varphi_x\right)\frac{dy}{ds} + \varphi_0' r + \frac{\partial \bar{w}}{\partial s}\right] + \varphi_0' \cdot n \tag{2}$$

with r being the component of $\mathbf{R}$ along $\mathbf{n}$ direction (Figure 1b). It should be noted that the term $\varphi_0'(z)\,n$ in Equation (2) corresponds to the torsional strain according to De Saint Venant's theory for pure torsion.

Moreover, according to Roberts and Al-Ubaidi [1], the torsional rotation $\varphi_0(z)$ is assumed to be the sum of:

- a rotation $\varphi_{0,w}(z)$ associated with axial warping and negligible shear strains;
- a rotation $\varphi_{0,s}(z)$ associated with shear strains $\gamma_{tz} = 2\varepsilon_{tz}(0, s, z)$ in the middle surface.

Consequently, the infinitesimal shear strain component on the cross-section middle line $\varepsilon_{tz}(0,s,z)$ can be rearranged as follows:

$$\varepsilon_{tz}(0,s,z)=\varepsilon_{tz}^{(0,w)}+\varepsilon_{tz}^{(0,s)}=\frac{1}{2}\left(\varphi'_{0,w}r+\frac{\partial\overline{w}}{\partial s}\right)+\frac{1}{2}\left[\left(u'_0-\varphi_y\right)\frac{dx}{ds}+\left(v'_0+\varphi_x\right)\frac{dy}{ds}+\varphi'_{0,s}r\right]. \tag{3}$$

By assuming infinitesimal shear strains due to the warping to be negligible, $\varepsilon_{tz}^{(0,w)}\cong 0$, it follows that:

$$\frac{\partial\overline{w}}{\partial s}=-\varphi'_{0,w}r \quad\Rightarrow\quad \int_M^P\frac{\partial\overline{w}}{\partial s}ds=-\int_M^P\varphi'_{0,w}rds \quad\Rightarrow\quad \overline{w}(s,z)=w_0(z)-\varphi'_{0,w}\omega, \tag{4}$$

where $w_0(z)$ is the displacement of the origin M along the z axis and $\omega(s)$ is the sectorial area, given by:

$$\omega(s)=\int_0^s r\,ds\,. \tag{5}$$

According to the aforementioned hypotheses, the non-zero Green-Saint Venant strain components in the local reference frame $\{\mathrm{P},\mathbf{n},\mathbf{t},\mathbf{k}\}$ result in the following:

$$\begin{aligned}
&H_{zz}=\varepsilon_{zz}+\frac{1}{2}\left[\nabla\mathbf{u}^{\mathrm{T}}\nabla\mathbf{u}\right]_{zz}=\\
&=\left[(y-y_M)\varphi'_x-(x-x_M)\varphi'_y-\omega(s)\varphi''_{0,w}+w'_0\right]+\\
&+\frac{1}{2}\left[u'^2_0+v'^2_0-(y-y_0)u'_0\varphi'_0+(x-x_0)v'_0\varphi'_0+\left(r^2+p^2\right)\varphi'^2_0+\right.\\
&\left.+(y-y_M)^2\varphi'^2_x+(x-x_M)^2\varphi'^2_y+\omega(s)^2\varphi''^2_{0,w}+w'^2_0\right]+\\
&+\left[-(x-x_M)(y-y_M)\varphi'_x\varphi'_y-\omega(s)(y-y_M)\varphi''_{0,w}\varphi'_x+\omega(s)(x-x_M)\varphi''_{0,w}\varphi'_y+\right.\\
&\left.+(y-y_M)w'_0\varphi'_x-(x-x_M)w'_0\varphi'_y-\omega(s)\varphi''_{0,w}w'_0\right],
\end{aligned} \tag{6a}$$

$$H_{tz} = \varepsilon_{tz} + \frac{1}{2}\left[\nabla \mathbf{u}^{\mathrm{T}} \nabla \mathbf{u}\right]_{tz} =$$

$$= \frac{1}{2}\left[\left(u_0' - \varphi_y\right)\frac{dx}{ds} + \left(v_0' + \varphi_x\right)\frac{dy}{ds} + \varphi_{0,s}' r\right] + \varphi_0'\, n +$$

$$+ \frac{1}{2}\frac{dx}{ds}\left[v_0'\varphi_0 + (x - x_0)\varphi_0\,\varphi_0' - \frac{1}{2}\left(y - y_M\right)\varphi_y\varphi_x' + \left(x - x_M\right)\varphi_y\varphi_y' + \omega(s)\varphi_y\varphi_{0,w}'' - \varphi_y w_0'\right] + \tag{6b}$$

$$+ \frac{1}{2}\frac{dy}{ds}\left[-u_0'\varphi_0 + (y - y_0)\varphi_0\,\varphi_0' + \frac{1}{2}\left(y - y_M\right)\varphi_x\varphi_x' - \left(x - x_M\right)\varphi_x\varphi_y' - \omega(s)\varphi_x\varphi_{0,w}'' + \varphi_x w_0'\right] +$$

$$- \frac{1}{2} r\left[\left(y - y_M\right)\varphi_{0,w}'\varphi_x' - \left(x - x_M\right)\varphi_{0,w}'\varphi_y' - \omega(s)\varphi_{0,w}'\varphi_{0,w}'' + \varphi_{0,w}' w_0'\right].$$

The weak form of the equilibrium equations is given by the principle of virtual displacements:

$$\delta W = \delta W_{\text{int}} + \delta W_{\text{ext}} = 0\,. \tag{7}$$

In Equation (7), δW_{int} and δW_{ext} are respectively the internal strain energy and work of the externally applied loads:

$$\delta W_{\text{int}} = \int_{\Omega} \delta H_{ij} T_{ij}\, dV\,, \tag{8a}$$

$$\delta W_{\text{ext}} = \int_0^L q(\mathrm{z})\delta w_0\, dz + \int_0^L p(z)\delta u_0\, dz + \sum_{i=1}^{n} Q_i \delta\Delta_i\,. \tag{8b}$$

where Ω is the region occupied by the beam, L the beam length, and H_{ij} and T_{ij} the respective components of the Green-Saint Venant strain tensor and the stress tensor with δ being the symbol of variation; $q(z)$ is the distributed transverse load per unit length; $p(z)$ is the distributed axial load per unit length; Q_i are the generalized nodal forces and $\delta\Delta_i$ the corresponding virtual displacements.

It is worth noting that by integrating the internal work on the cross-section of the beam, it is possible to express the equation as a function of the variable z so as to obtain a one-dimensional model.

3. Finite Element Model

Let us consider a finite element discretization of the beam axis into a collection of two nodes Hermitian elements. With reference to the *e-th* finite element,

$$\mathbf{\Delta}^{(e)}(\xi)=\left[\Delta_i^{(e)}(\xi)\right]^{\mathrm{T}}=\left[u_0(\xi)\quad v_0(\xi)\quad w_0(\xi)\quad \varphi_x(\xi)\quad \varphi_y(\xi)\quad \varphi_{0,w}(\xi)\quad \varphi_{0,s}(\xi)\right]^{\mathrm{T}}, \tag{9}$$

is the vector collecting the independent displacement components as a function of the natural coordinate ξ of the generic cross-section, referred to the element of length $l^{(e)}$.

This discretization allows us to express the non-zero Green-Saint Venant strain components (6 a,b) in matrix form, as a function of 14 nodal displacement and their first derivatives vectors $\mathbf{\Delta}^{(e)}$:

$$\mathbf{H}^{(e)}=\mathbf{B}^{(e)}(\mathbf{\Delta}^{(e)})\mathbf{\Delta}^{(e)} \tag{10}$$

where

$$\mathbf{H}^{(e)}=\left[H_{zz}\quad H_{tz}\right]^{\mathrm{T}}, \tag{11}$$

$$\mathbf{\Delta}^{(e)}=\left[u_{0i},v_{0i},w_{0i},\varphi_{xi},\varphi_{yi},\varphi_{0,si},\varphi_{0,wi},u'_{0i},v'_{0i},w'_{0i},\varphi'_{xi},\varphi'_{yi},\varphi'_{0,si},\varphi'_{0,wi}\right]^{\mathrm{T}}\ (i=1,2) \tag{12}$$

and $\mathbf{B}^{(e)}$ is a matrix that is function of $\mathbf{\Delta}^{(e)}$ and includes the Hermite shape functions.

Let us assemble the components of the stress tensor corresponding to the aforementioned strain components in the following vector:

$$\mathbf{T}^{(e)}=\left[\sigma_{zz}\quad \tau_{tz}\right]^{\mathrm{T}}. \tag{13}$$

By considering transversally isotropic constitutive behavior and according to the beam strain regime, the following constitutive law can be adopted:

$$\mathbf{T}^{(e)}=\mathbf{C}\,\mathbf{H}^{(e)}, \tag{14}$$

where $\mathbf{C}$ is a matrix collecting the material properties:

$$\mathbf{C} = \begin{bmatrix} E_{zz} & 0 \\ 0 & G_{tz} \end{bmatrix}. \tag{15}$$

Although a transversely isotropic material is, in general, defined by 5 parameters, according to the kinematic assumptions previously introduced, we can refer to only two parameters. In detail, E_{zz} is the longitudinal modulus of elasticity and G_{tz} is the shear modulus of elasticity in the cross section plane.

The finite element discretization of the virtual strain energy and external work allows one to define the non-linear stiffness matrix of the generic finite element, $\mathbf{K}^{(e)}(\mathbf{\Delta}^{(e)})$, and the vector collecting the generalized nodal forces of the element, $\mathbf{F}^{(e)}$. By assembling them into the global non-linear stiffness matrix, $\mathbf{K}(\mathbf{\Delta})$, and into the global force vector, $\mathbf{F}$, respectively, the non-linear problem (7) can be expressed on the beam domain as follows:

$$\left[\mathbf{K}(\mathbf{\Delta})\mathbf{\Delta} - \mathbf{F}\right] \cdot \delta\mathbf{\Delta} = \mathbf{0} \qquad \forall \delta\mathbf{\Delta}. \tag{16}$$

The non-linear set of Equation (16) can be solved by an incremental-iterative procedure controlled by load and based on the Newton-Raphson method. The incremental procedure can be adopted starting with perfectly straight or geometrically imperfect beams.

4. Numerical Results

The numerical investigation presented here deals with the non-linear behavior of glass PFRP thin-walled I-beams.

The profiles considered are constrained at the ends by torsional restraints, that allow only the rotations about *x* and *y* axes. They are subject to a uniformly distributed transverse load in the

(*y*,*z*) plane and applied to the middle line of the upper flange (Figure 2). The cross-section has the following geometrical properties: $h = 200$ mm , $b = 100$ mm , and $t_f = t_w = 10$ mm (Figure 3).

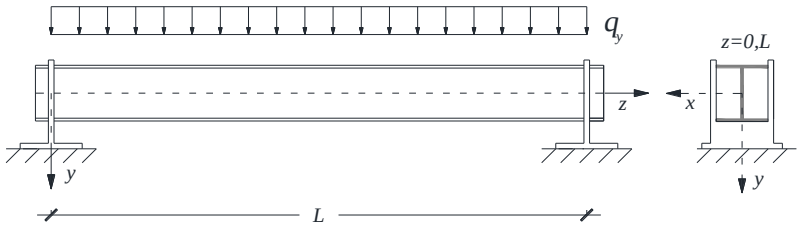

Figure 2 – Static scheme of PFRP analyzed beam

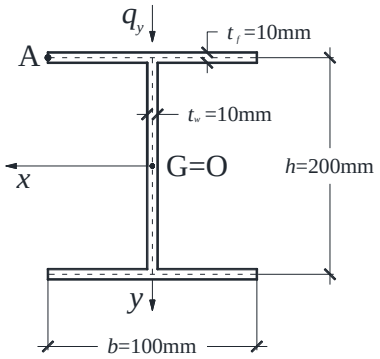

Figure 3 – Cross-section of PFRP analyzed beam

Considering the cross-section as an isotropy plane, the material is characterized by the longitudinal elastic modulus E_{zz} =23.0 GPa and shear transverse modulus G_{tz} =3.0 GPa. The choice of mechanical properties used here relates to the typical values given by producers with reference to glass PFRP beams.

With the aim of investigating the non-linear behavior of such profiles, the numerical analysis is conducted on geometrically imperfect I-beams, while considering three different span lengths, *L*, and three different initial defects. The assumed geometrical imperfection corresponds to a quadratic out-of-straightness, whose maximum value of lateral displacement is equal to *f* (Figure 4). This type of defect can typically be found in current all-PFRP structures due to the profile manufacturing process and/or on-site mounting.

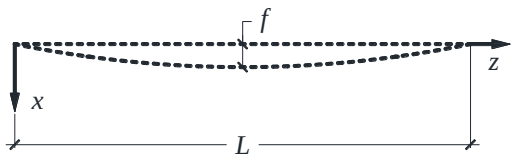

Figure 4 – Out-of-straightness of the imperfect beam.

Table 1 reports, for each of the case analyzed (I1, I2, I3), the beam length, the *h/L* ratio, the value of the reference buckling under the uniformly distributed load, $q_{CR,PB}$, calculated using the present model on almost perfect beams (*f/L* = 0.00001), the maximum amplitude of imperfections, f, the *f/L* ratio and the number of adopted elements, N_e. These values are lower than the maximum magnitude allowed by ASTM D3917-11 [17], which is equal to 0.00417 (*L*/240).

Table 1 – Case studies geometrical properties, buckling loads for perfect beams and number of elements adopted in FEM analyses.

ID	L [mm]	h	h / L	f [mm]	f / L	$q_{CR,PB}$ [N/mm]	N_e
I1	1000	200	1/5	1	0.001	300.10	15
				2	0.002		
				4	0.004		
I2	2000	200	1/10	2	0.001	20.36	20
				4	0.002		
				8	0.004		
I3	3000	200	1/15	3	0.001	4.10	25
				6	0.002		
				12	0.004		

Let us first consider the effect of imperfections on the I2 beam according to the present theory.

Figures 5 and 6 show load mid-span cross-sectional plane centroidal displacements components obtained. More specifically, they refer respectively to the centroid horizontal and

vertical displacements, hereafter denoted by the symbols u_G, and v_G. The straight lines depicted in Figure 6 also show the behavior of the beam in bending considering either Timoshenko or Eulero-Bernoulli classical theories, without including nonlinear effects (Figure 6). Since no lateral loads are applied, a linear analysis does not allow for horizontal displacements in the cross section centroid (Figure 5).

According to the present theory, two stages can be clearly distinguished in the load paths: the first characterized by pre-buckling behavior and the second by buckling and initial post-buckling behavior. It should be noted how the initial imperfection can significantly affect the lateral displacement, as the effect of nonlinearities appears very relevant when the higher values of *f/L* are considered. In fact, the displacement corresponding to the transition between the two stages is about three times greater when an imperfection of *f/L* = 0.004 rather than *f/L* = 0.001 is considered. On the contrary, the initial imperfection may only slightly influence the maximum vertical displacement.

Figures 7, 8, 9 show the normalized distributed load, given by the ratio between the uniformly distributed load and the buckling load (Table 1), against the torsional rotation φ_0 exhibited by the I2 beam. In these Figures, each referring to a different magnitude of the imperfection, the results of the present theory are compared with a linear analysis performed according to both Vlasov's and Saint Venant's classical theories.

According to Vlasov's theory, both primary and secondary torsion are taken into account whereas Saint Venant's theory is not able to take into account for secondary torsion effects. Both theories neglect the effects of shear deformability. It is well known that Saint Venant theory is not adequate to evaluate torsional behavior of thin walled beams as it lead to underestimate its torsional stiffness.

According to present theory, as shown in Figures 7, 8 and 9, pultruded FRP thin walled beams may experience torsional stiffness significantly lower than what is considered by Vlasov's theory. This happens not only for high values of the load, when the effects of the nonlinearities are significant, but also in the initial linear branch, due to the effects of shear deformability. Moreover, this effect is all the more significant the higher is the initial degree of imperfection considerer (cf. Figures 7, 8 and 9).

Further simulations were carried out with the aim of identifying the uniformly distributed load corresponding to a suitable deformation limit for different values of imperfection. Due to the lack of specific requirements suggested for PFRPs, the maximum value of displacement was assumed to be equal to $L/400$ in accordance with the deformation limits commonly suggested for steel structures in international codes and guidelines.

Let us define d_{G} and d_{A} as the magnitude of the displacement vectors respectively exhibited by the beam at the centroid, G, and at the end point of the flange middle line, A, both being considered at middle span cross-section (Figure 3). The normalized distributed load, given by the ratio between the uniformly distributed load and the buckling load (Table 1) are depicted in relation to the normalized displacements d_{G}/L and d_{A}/L in Figures 10, 11, and 12. More specifically, each figure refers to a given length (L=1000 mm, Figure 10; L=2000 mm, Figure 11; L=3000 mm, Figure 12) and shows the numerical predictions computed in relation to the three different amplitudes of initial imperfection. In these figures, the perfect beam linear behavior (PBLB) and serviceability limit deflection ($L/400$) are represented. Such diagrams show that the effects of nonlinearities may be relevant in terms of beam deformability, as the span length and initial imperfection tend to increase. Furthermore, due to thin-walled geometry, the displacements

of point A are generally much more relevant than those of point G because of the torsional rotation contributions.

These results highlight that the initial defect does not significantly affect the displacements in short-span beams (*h/L*=1/5), as the load path shown is almost linear, although high imperfections are considered (Figure 10). On the contrary, the intermediate-length beams (*h/L*=1/10) are characterized by a non-linear load path, which influences the initial imperfection (Figure 11). This behavior is much more marked in slender beams (*h/L*=1/15), where the stiffness shows a strong decrease even for the low values of external loads (Figure 12).

Let us introduce the value q_S corresponding to a displacement d_A equal to the limit deflection *L*/400: such value can be considered as the load at the serviceability limit state. Table 2 reports the percentage differences, Δq_S, between the serviceability load exhibited by each imperfect beam, $q_{S,IB}$, and that obtained by a linear analysis on the perfect beam, $q_{S,PB}$.

Table 2 – Comparison between serviceability load of perfect and imperfect beams.

ID	$q_{S,PB}$ [N/mm]	f / L	$q_{S,IB}$ [N/mm]	Δq_S %
I1	59.43	0.001	57.17	-1
		0.002	54.74	-5
		0.004	49.81	-14
I2	11.82	0.001	9.91	-15
		0.002	8.32	-29
		0.004	6.26	-46
I3	3.93	0.001	2.60	-34
		0.002	2.05	-48
		0.004	1.46	-63

As expected, the magnitude of Δq_S increases as the beam slenderness and imperfection amplitude increase. Moreover, it can be observed that the influence of defect is much more relevant when higher spans are considered since the limit deflection 1/400 corresponds to a highly non-linear regime (q_S is quite close to $q_{CR,PB}$). In particular, the case I1 (short-span beams) shows that the results for the serviceability load prediction are only 1% to 14% lower than the perfect beam reference value for the considered defect range. In contrast, decreases in q_S of up to 46% and 63% are observed in cases I2 (medium-length beams) and I3 (slender beams), respectively.

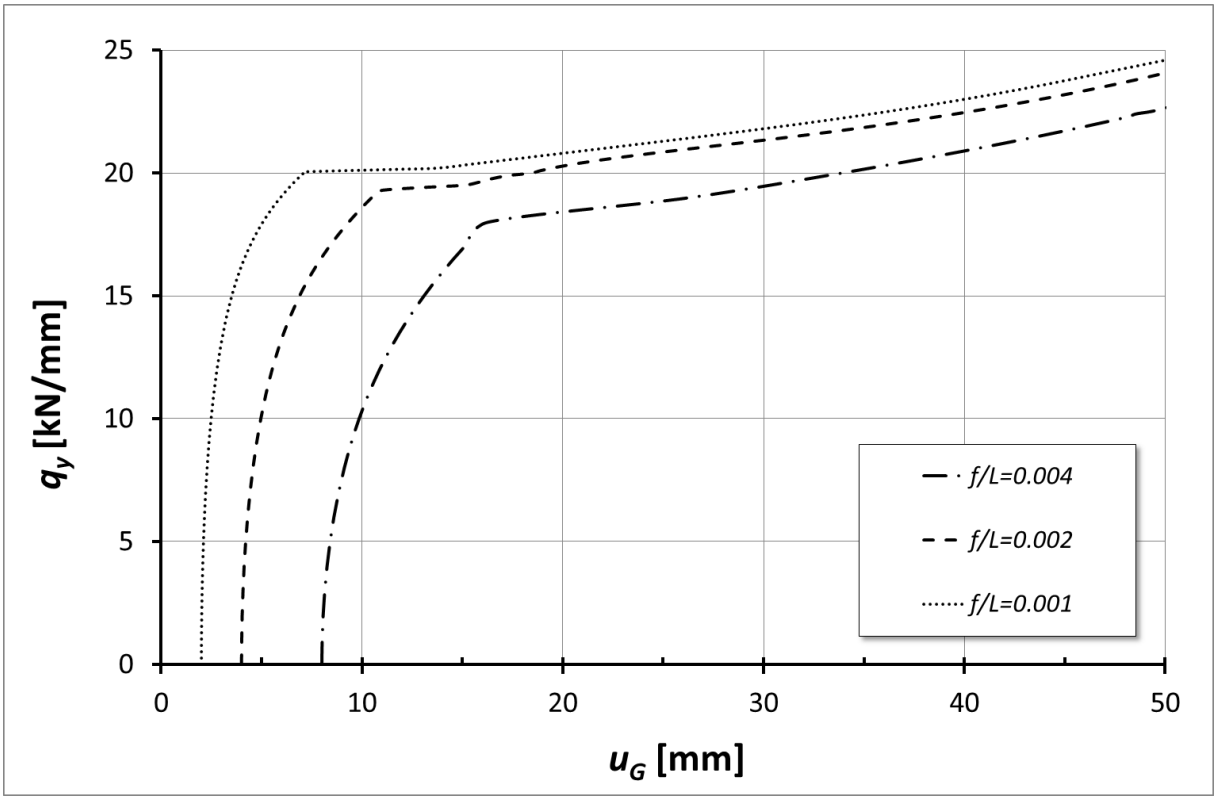

Figure 5 – Uniformly distributed load q_y versus the displacement component u_G (beam I2).

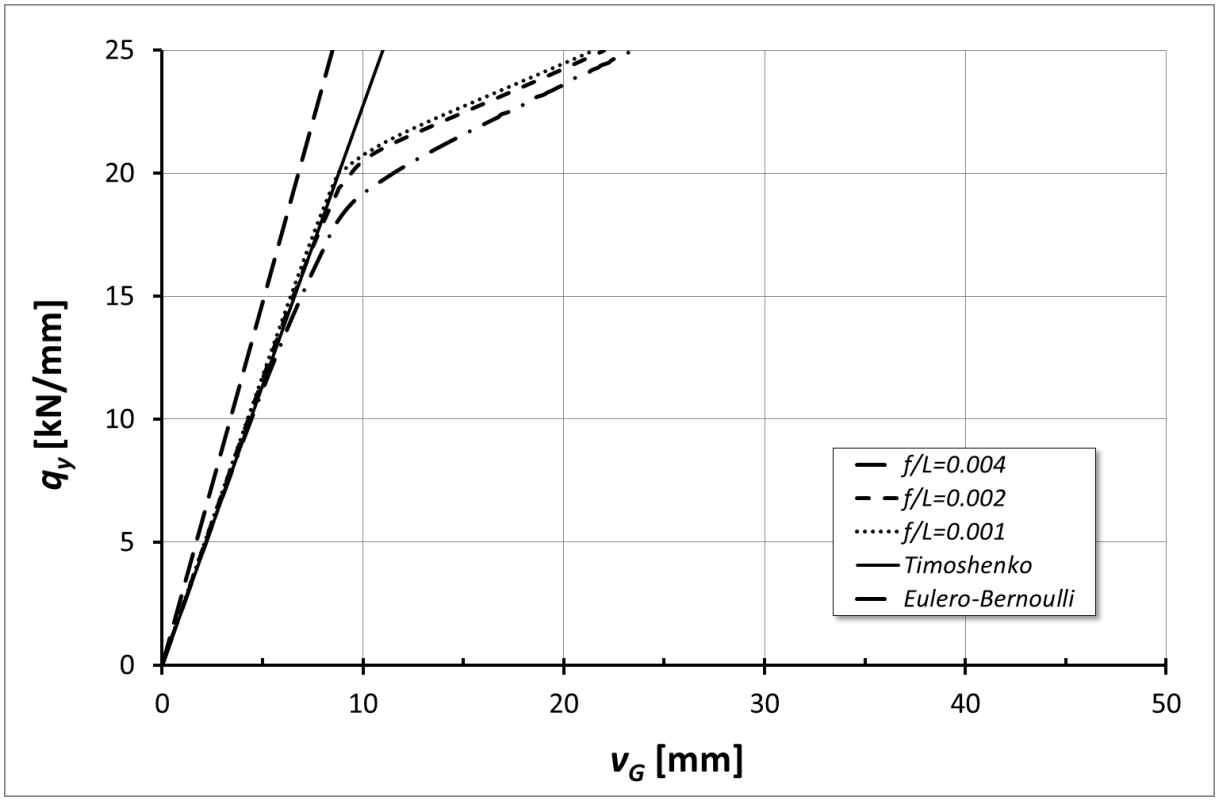

Figure 6 – Uniformly distributed load q_y versus the displacement component v_G (beam I2).

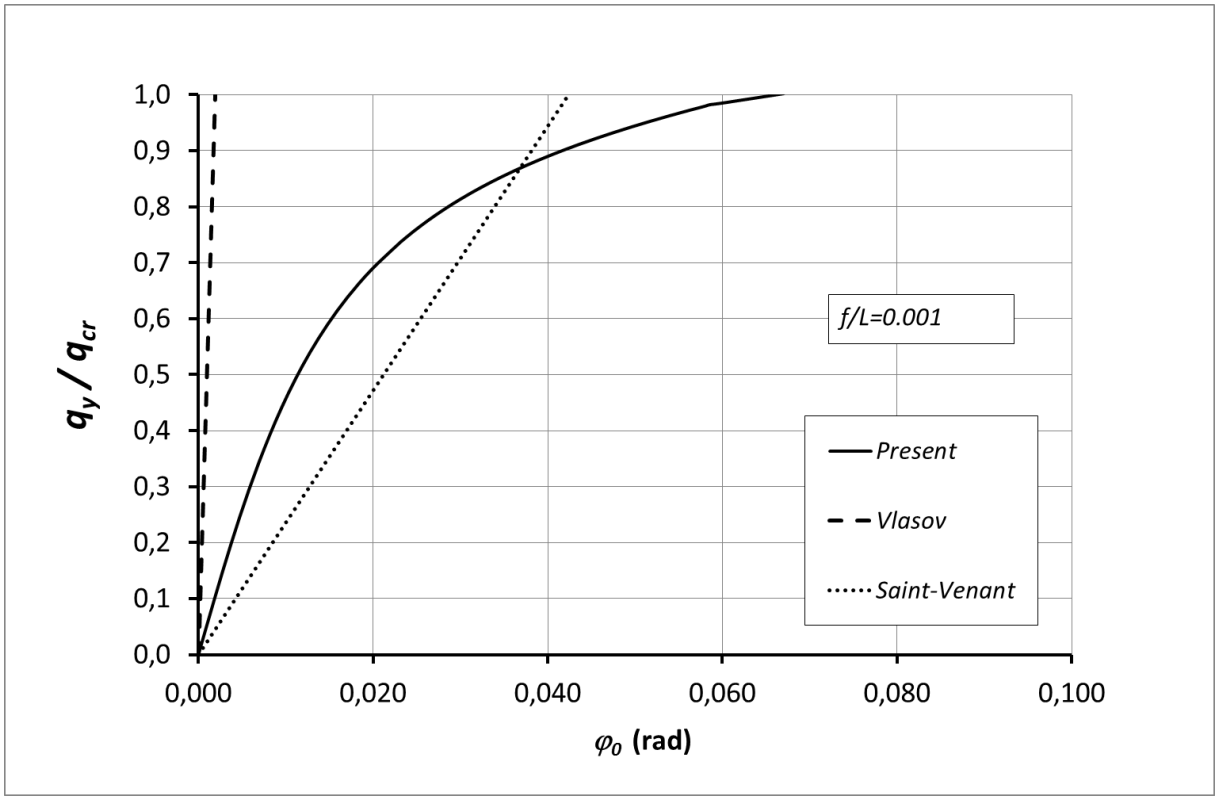

Figure 7 – Normalized uniformly distributed load versus φ_0 (beam I2, f/L =0.001)

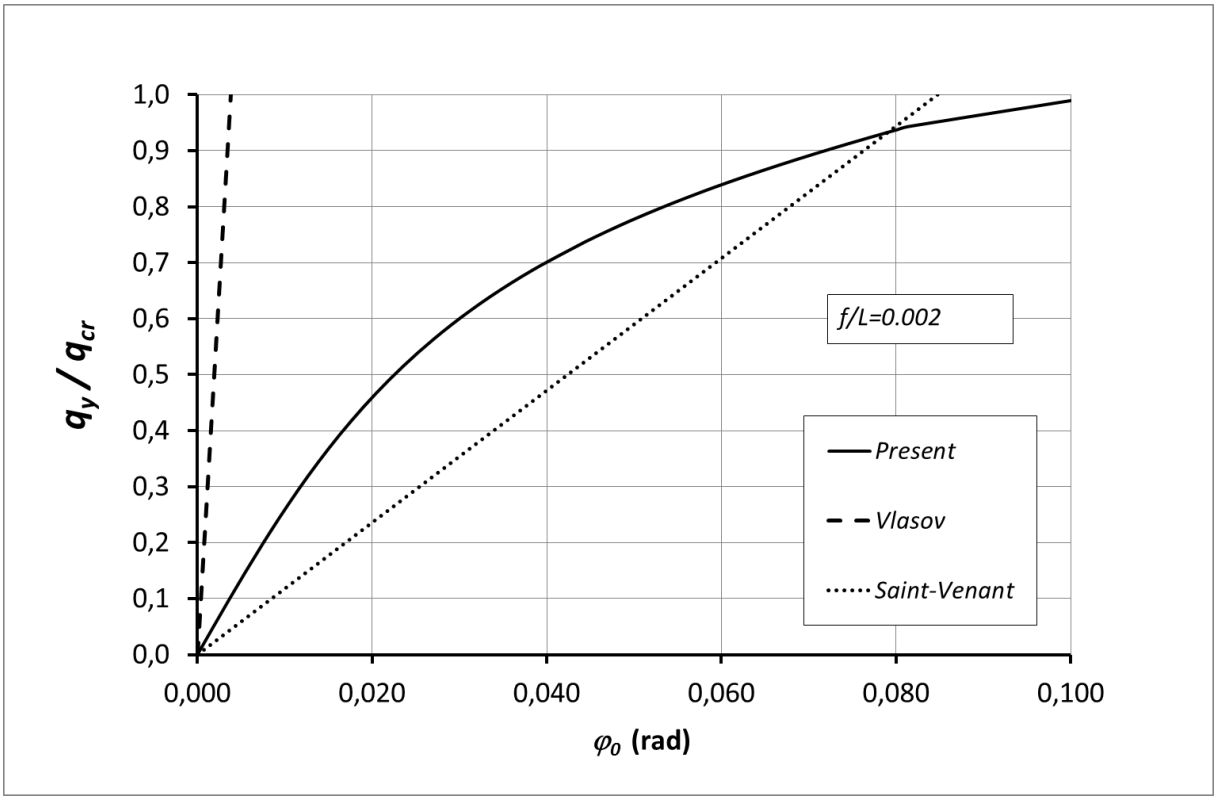

Figure 8 – Normalized uniformly distributed load versus φ_0 (beam I2, f/L =0.002)

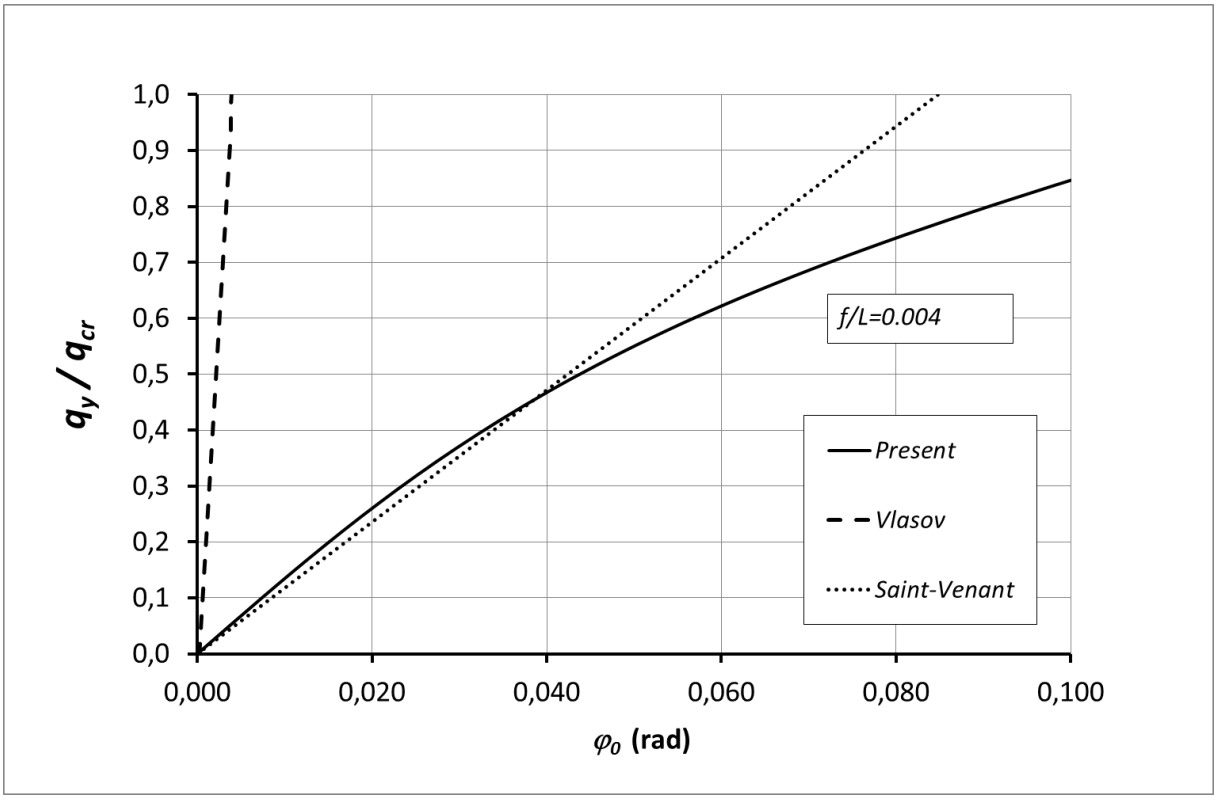

Figure 9 – Normalized uniformly distributed load versus φ_0 (beam I2, f/L =0.004)

(a)

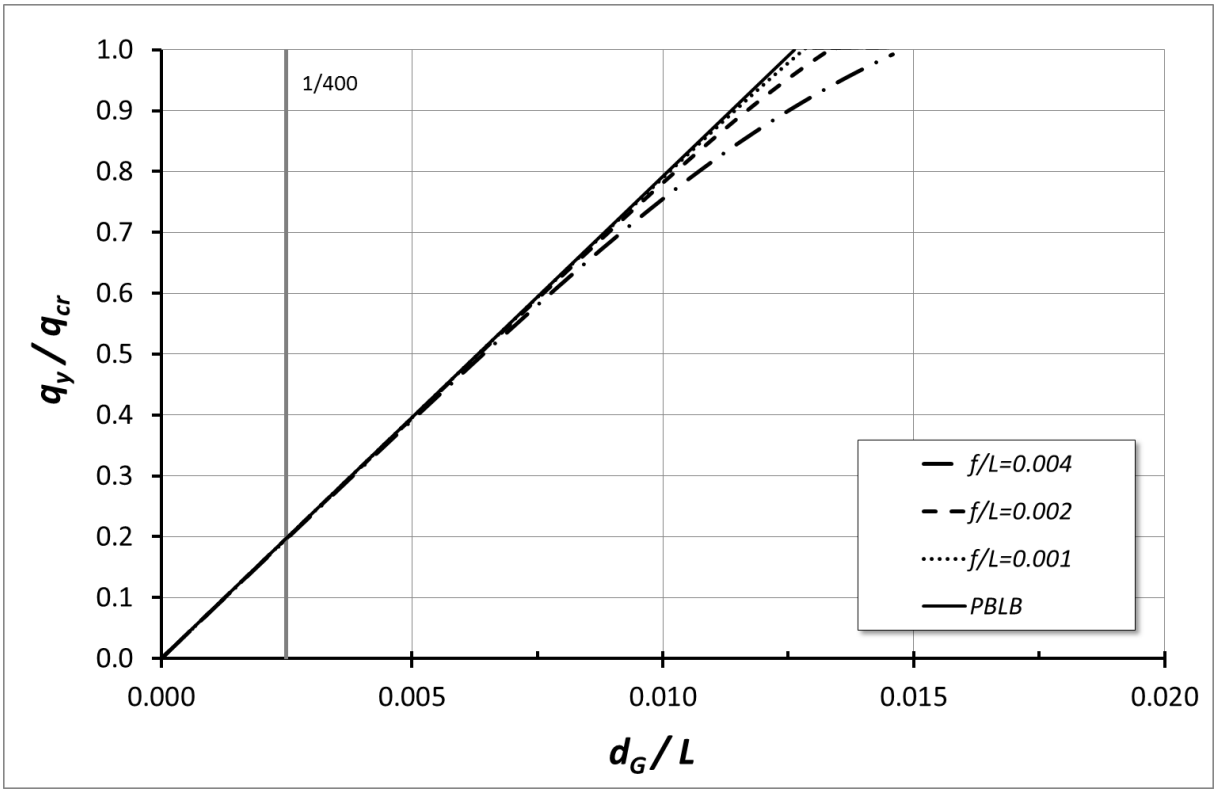

(b)

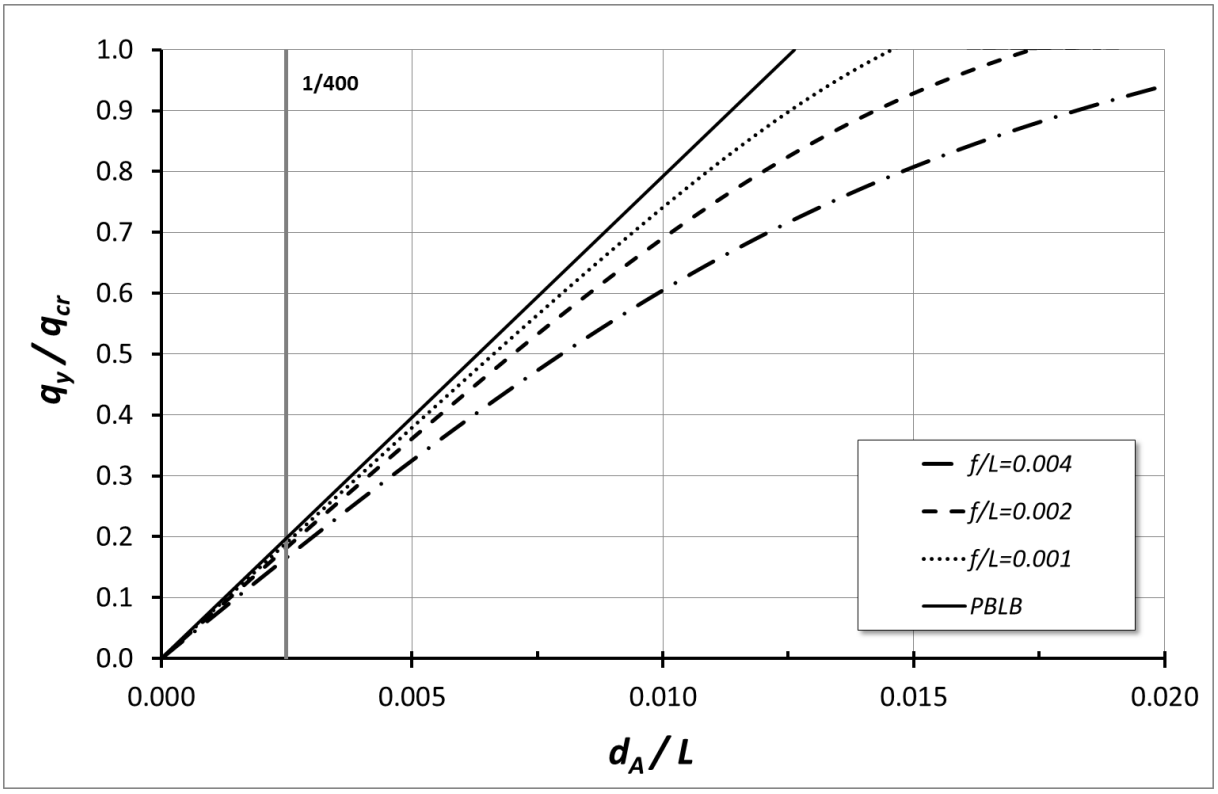

Figure 10 – Beam I1: a) Normalized uniformly distributed load versus d_G; b) Normalized uniformly distributed load versus d_A.

(a)

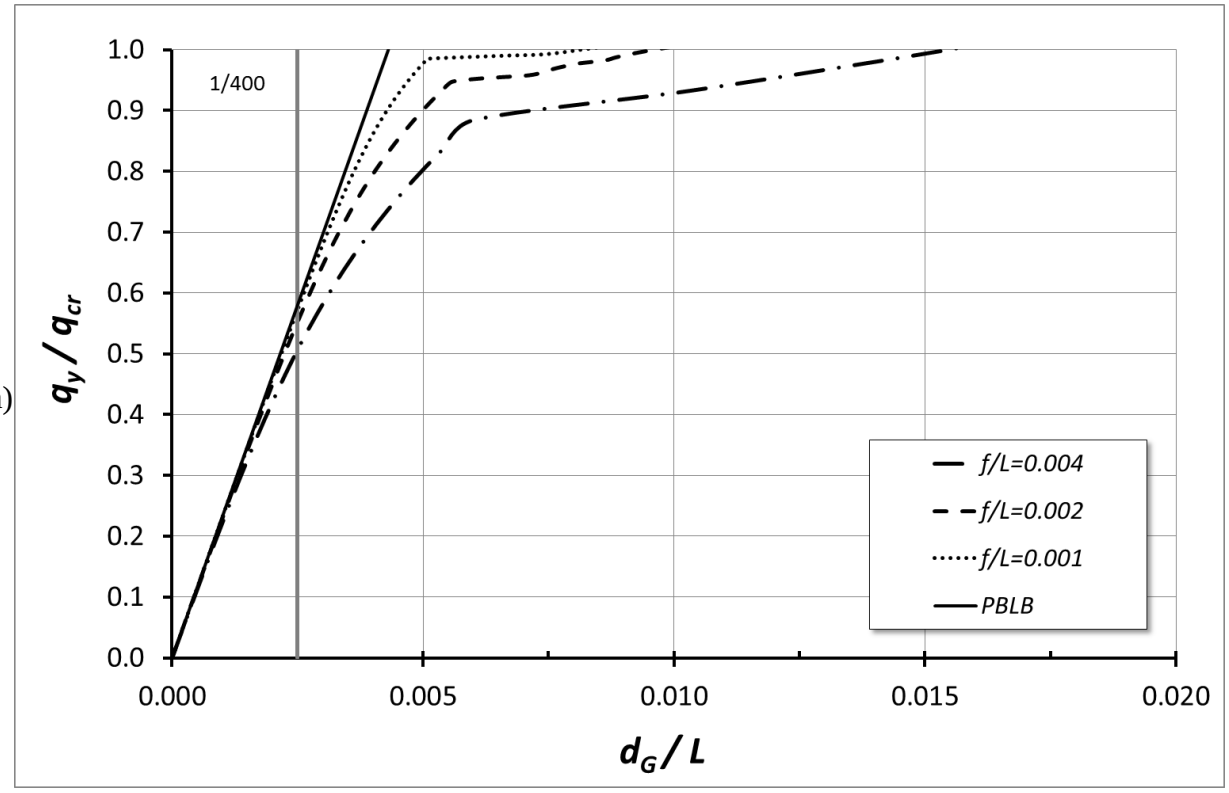

(b)

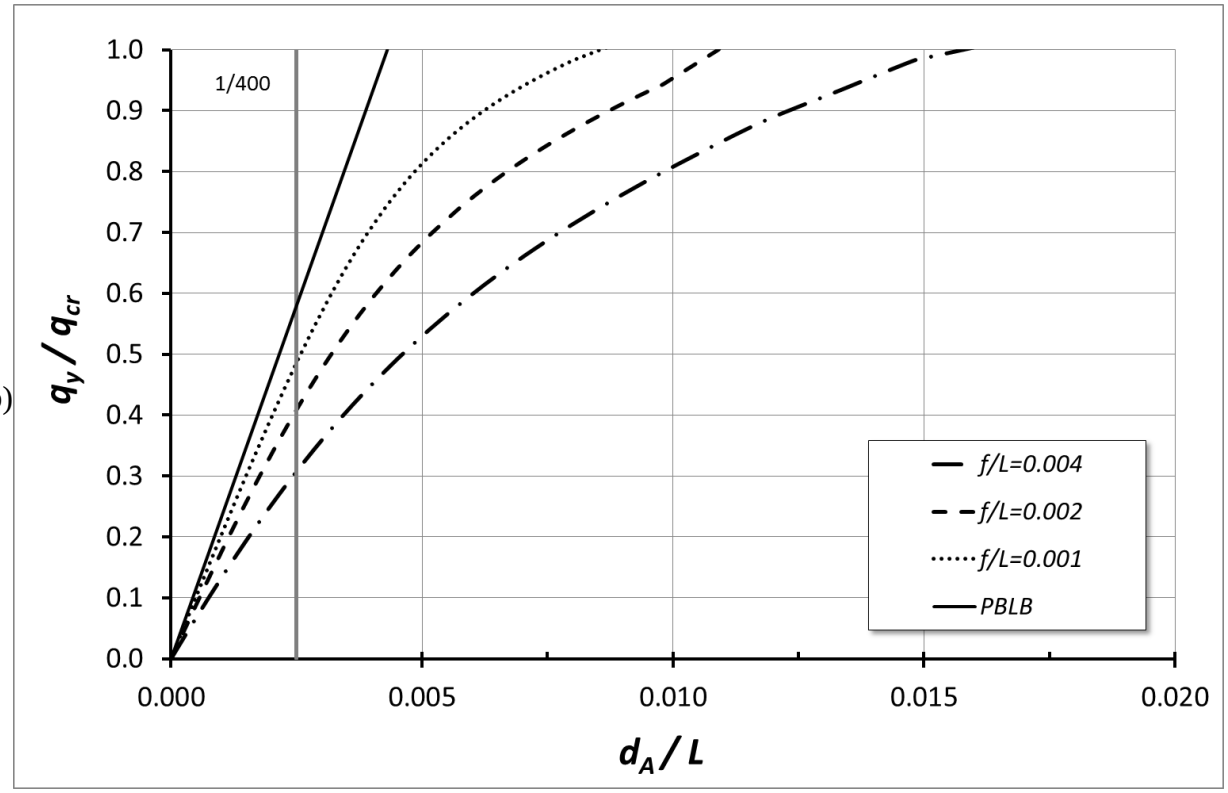

Figure 11 – Beam I2: a) Normalized uniformly distributed load versus d_G; b) Normalized uniformly distributed load versus d_A.

(a)

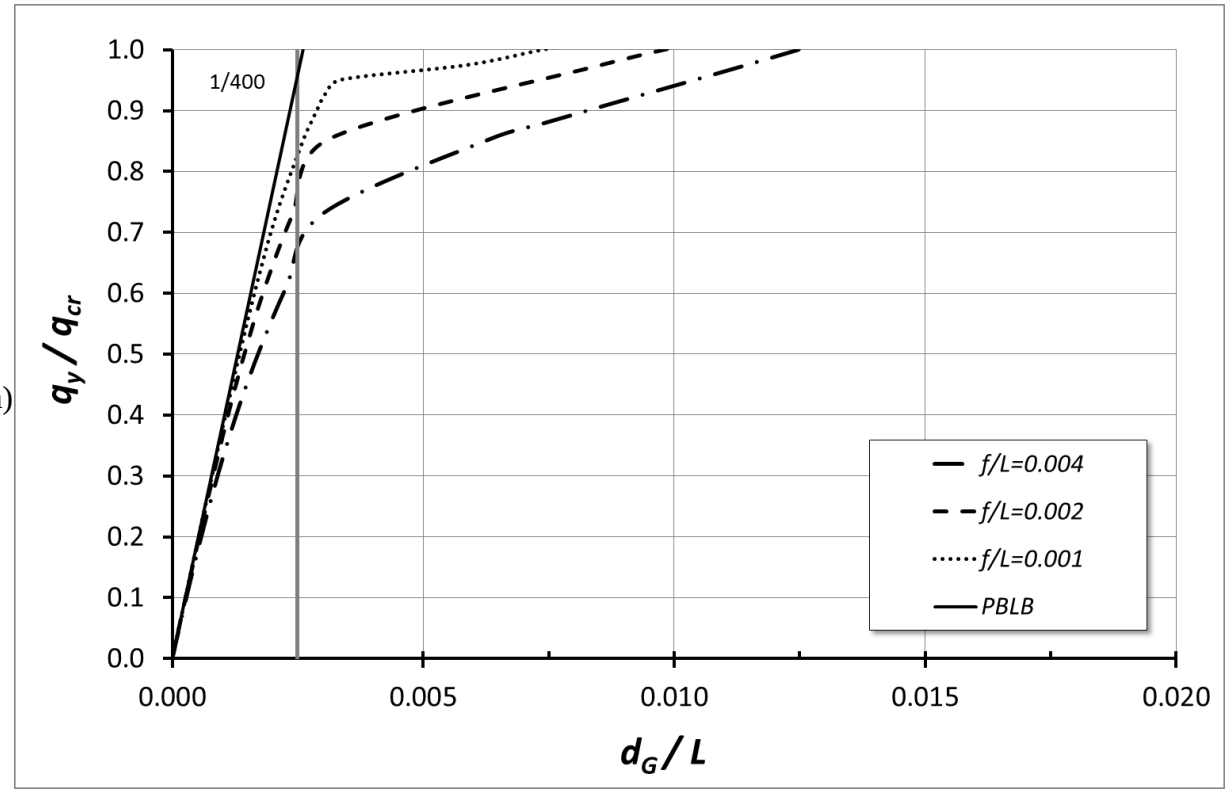

(b)

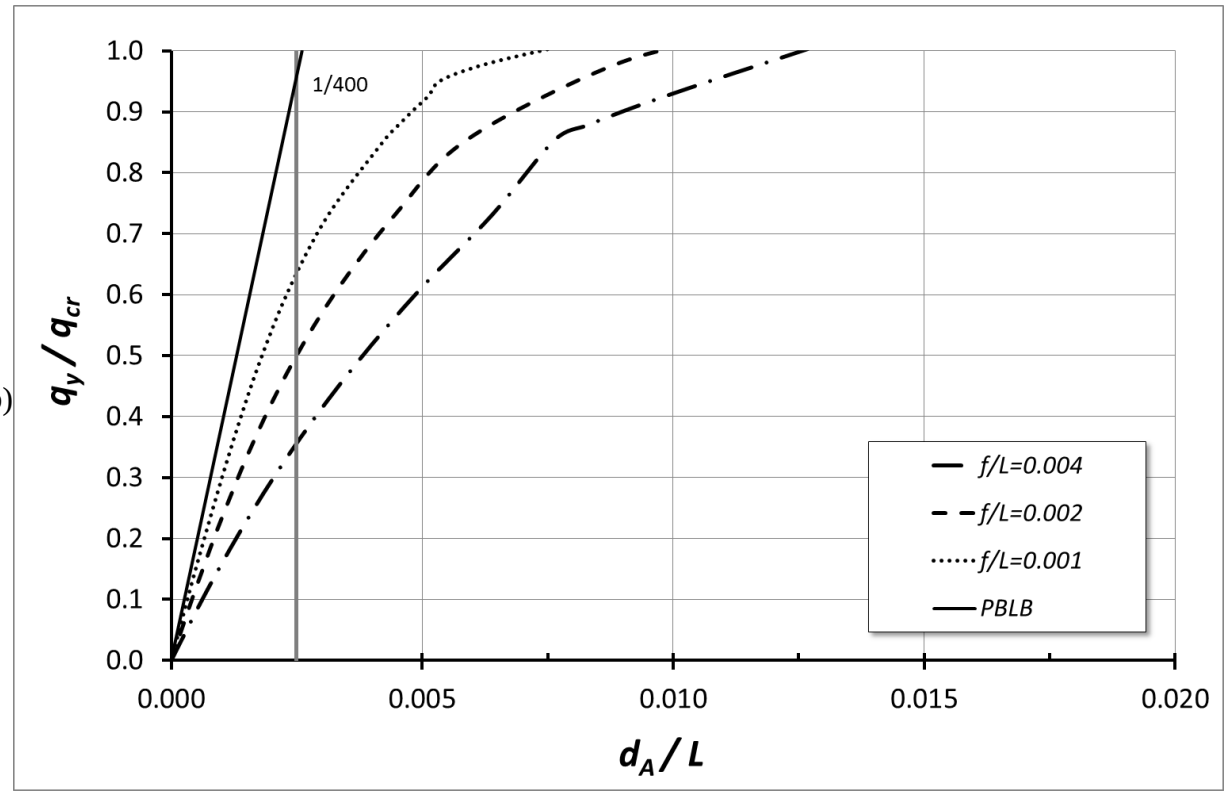

Figure 12 – Beam I3: a) Normalized uniformly distributed load versus d_G; b) Normalized uniformly distributed load versus d_A.

5. Conclusions

This paper presented a non-linear mechanical model capable of predicting the pre-buckling behavior of PFRP imperfect beams with open thin-walled cross-sections. The model was formulated by assuming the material to be linear-elastic, homogeneous, and transversely isotropic, and considering the contribution of shear deformability on geometric non-linearity.

A numerical investigation conducted by means of a FEM code, as proposed by the authors based on this mechanical model, was also shown. The analysis was conducted on geometrically imperfect I-beams, considering three different span lengths and three different amplitudes of the initial out-of-straightness imperfections.

The results show the relevance of nonlinearities and thin-walled geometry on beam deformability, especially when slender beams are considered. Furthermore, the maximum displacements of the flange are generally much more relevant than those of the cross-section centroid because of the torsional rotation contributions.

As expected, the study also highlighted that:

- the load-deflection curve of short-span beams is almost linear, although high imperfections are considered;
- slender beams exhibit a marked non-linear behavior, with the significant influence of the initial imperfection;
- the load at the serviceability limit state in beams with defects was significantly lower than the load exhibited by an equivalent perfect beam, especially when high slenderness and imperfection amplitudes are considered.

The present study highlights the effectiveness of the proposed mechanical model for analyzing the pre-buckling behavior of PFRP beams in order to satisfy serviceability design requirements at a reasonable computational cost. On the basis of the numerical results, it should be noted that due

to the effect of imperfections, the decrease of loads that can be assigned to PFRP structural elements can be very significant. Therefore, the effect of geometric nonlinearity on their mechanical behavior must be mandatory taken into account by international codes and guidelines.

Acknowledgements

The authors gratefully acknowledge the Italian Department of Civil Protection (DPC) for the financial support received (RELUIS III 2014-2017 grant).

References

[1] Roberts, T.M., and Al-Ubaidi, H. (2001). "Influence of shear deformation on restrained torsional warping of pultruded FRP bars of open cross-section". Thin-Walled Structures. 39, 395-414.

[2] Sapkas A., and Kollar L.P., (2002). "Lateral-torsional buckling of composite beams." Int. J. Solids Struct., 39, 2939–2963.

[3] Machado, S.P., and Cortinez, V.H., (2005). "Lateral buckling of thin-walled composite bisymmetric beams with prebuckling and shear deformation." Eng. Struct., 27, 1185–1196.

[4] Ascione, L., Giordano, A., and Spadea, S. (2011). "Lateral buckling of pultruded FRP beams."Composites Part B: Engineering, 42 (4), 819–824.

[5] Ascione, L., Berardi, V.P., Giordano, A., Spadea, S. (2013) Local buckling behavior of FRP thin-walled beams: A mechanical model. Composite Structures, 98, pp. 111-120.

[6] Ascione, L., Berardi, V.P., Giordano, A., and Spadea, S. (2013). "Buckling failure modes of FRP thin-walled beams." Composites Part B: Engineering, 47, pp. 357-364.

[7] Ascione, L., Berardi, V.P., Giordano, A., Spadea, S. (2014) Macro-scale analysis of local and global buckling behavior of T and C composite sections. Mechanics Research Communications, 58, pp. 105-111.

[8] Fraternali, F., and Feo L., (2002). "On a moderate rotation theory of thin-walled composite beams." Compos. Part B Eng., 31, 141–158.

[9] Machado, S.P. (2010). "Non-linear stability analysis of imperfect thin-walled composite beams." International Journal of Non-Linear Mechanics, 45 (2), pp. 100-110.

[10] Mancusi, G., Feo, L. (2013) "Non-linear pre-buckling behavior of shear deformable thin-walled composite beams with open cross-section." Composites Part B: Engineering, 47, pp. 379-390.

[11] Vieira, R.F., Virtuoso, F.B.E., Pereira, E.B.R. (2013). "A higher order thin-walled beam model including warping and shear modes." International Journal of Mechanical Sciences, 66, pp. 67-82.

[12] Nguyen, T. T., Chan, T. M., and Mottram, J. T. (2013). "Influence of boundary conditions and geometric imperfections on lateral-torsional buckling resistance of a pultruded FRP I-beam by FEA." Compos. Struct., 100, 233–242.

[13] Fraternali, F., Spadea, S., Ascione, L. (2013) Buckling behavior of curved composite beams with different elastic response in tension and compression. Composite Structures, 100, pp. 280-289.

[14] Laudiero, F., Minghini, F., Tullini, N. (2014). "Buckling and postbuckling finite-element analysis of pultruded FRP profiles under pure compression." ASCE Journal of Composites for Construction, 18 (1).

[15] Ascione, F., and Mancusi, G. (2013) “The influence of the web-flange junction stiffness on the mechanical behaviour of thin-walled pultruded beams.” Composites Part B: Engineering, 55, pp. 599-606.

[16] Ascione, F. (2014). “Influence of initial geometric imperfections in the lateral buckling problem of thin walled pultruded GFRP I-profiles.” Composite structures, 112, 85-99.

[17] ASTM D3917-11. Standard Specification for Dimensional Tolerance of Thermosetting Glass-Reinforced Plastic Pultruded Shapes. ASTM International, 2011.